Accurate Photonic Analog-to-Digital Conversion

***Anatol Khilo*[1], *Cheryl M. Sorace*[1], *Jonathan R. Birge*[1], *and Franz X. Kärtner*[1,2]**

[1]Department of Electrical Engineering and Computer Science and Research Laboratory of Electronics, Massachusetts Institute of Technology, 77 Massachusetts Ave., Cambridge, MA 02139, USA, anatolykhilo@gmail.com, kaertner@mit.edu

[2]DESY-Center for Free-Electron Laser Science and Hamburg Univ., Notkestraße 85, D-22607 Hamburg, Germany

Abstract

Photonic analog-to-digital converters (ADCs) are attracting significant interest due to promise of overcoming the problem of aperture jitter and improving ADC performance level by orders of magnitude. This work examines several critical factors which define the accuracy of an optically-sampled wavelength-demultiplexed ADC built on a silicon chip using silicon photonic technology. These factors are the optical power-dependent shot noise, optical power-dependent nonlinearities due to two-photon and free-carrier absorption in silicon, and nonlinear transfer function of a silicon modulator. Ways to reduce the impact of these factors on ADC accuracy are considered.

1. Introduction

The interest to photonic ADCs is motivated by the prospect of using ultra-stable pulse trains available from mode-locked lasers to eliminate the problem of aperture jitter – a major problem on the way towards faster and more accurate ADCs [1]. The photonic ADC studied in this work is shown in Fig. 1. A low-jitter pulse train generated by a mode-locked laser passes through a dispersive fiber. This broadens the pulses temporally and creates continuous time-to-wavelength mapping within them so that different wavelengths correspond to different time moments [2]. A discrete version of the time-to-wavelength mapping can be created by wavelength-demultiplexing the pulse train into multiple sub-trains, applying differential delays, and recombining them into a single path, which results in a train of pulses with periodically repeating wavelengths [3, 4]. This pulse train is modulated by a modulator whose RF input $v(t)$ is the signal to be sampled. Thanks to time-to-wavelength mapping, the modulator effectively imprints the time dependence of $v(t)$ onto the optical spectrum. The optical signal is demultiplexed into N channels by a filter bank. Each channel is detected by a photodetector and digitized by an electronic ADC taking one sample per pulse. This sample represents the RF signal at the time moment defined by the time-to-wavelength mapping. The scheme with N channels increases the sampling rate over what is available in electronic ADCs by a factor of N as well as reduces the bandwidth requirements of photodetectors and electronic ADCs [2-4]. Some impressive results demonstrated with photonic ADCs built using discrete components include 9.8 bits for 0.77GHz [5], 7 bits for 10GHz [6], and 6-7 bits for 10GHz input signals [7]. The last two results were achieved with the time-stretch approach, where the modulated pulses are additionally stretched in time with dispersive fibers. The emerging silicon photonic technology promises integration of a photonic ADC on a single Si chip, turning photonic ADCs from bulky and costly prototypes into cheap, robust, mass-produced devices. This work analyzes the accuracy of integrated photonic ADCs as limited by shot noise, nonlinear Si effects, and modulator nonlinearity, and suggests ways to improve this accuracy.

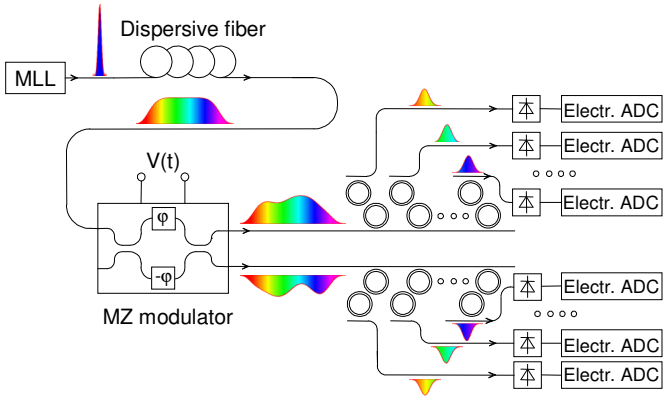

Fig. 1. Optically-sampled wavelength-demultiplexed photonic ADC, using microring resonators for wavelength demultiplexing.

978-1-4244-6051-9/11/$26.00 ©2011 IEEE

2. Optical Power and Silicon Nonlinearities

One of the main questions in the analysis of photonic ADCs is the optical power required for a given performance level. On one hand, high optical power is needed to improve the signal-to-noise ratio (SNR), on the other hand, high power can cause significant distortions due to nonlinearities in Si waveguides and photodetectors. The dependence of shot noise and silicon nonlinearity-induced distortions on optical power is analyzed below.

A fundamental limitation on photonic ADC performance is related to the fact that the number of photons in a classical optical pulse follows a Poisson statistics [8]: if the average number of photons in a pulse is N, the standard deviation of the photon number is $N^{1/2}$. The corresponding SNR of a pulse train modulated with a single-tone sinusoidal signal $\sin(\omega t)$ can be calculated as follows. The average number of photons per pulse is approximately $N(t)=0.5N_0\,[1+m\,\sin(\omega t)]$, where m is the modulation index and N_0 is the average photon number at the input of the modulator. The electrical signal at frequency ω generated by a photodetector is $\sim 0.5N_0\,m\,\sin(\omega t)$; the average power of this signal is $\sim N_0^2 m^2/8$. The electrical noise power, from Poisson statistics, is the average of $N(t)$, which is $N_0/2$. Therefore, SNR = $N_0\,m^2/4$. Note the steep scaling of the SNR with modulation index m, which occurs because the power of the "useful" signal scales as m^2, while the noise power is independent on m. Assuming 50% modulation, to achieve ENOB=8.0, the number of photons per pulse must be $1.5\cdot 10^6$ (energy of 200 fJ at 1550 nm optical wavelength, or average power of 0.2mW assuming a 1 GHz pulse train). The pulse energy must be increased by a factor of 4 per each additional bit.

As optical power is increased to improve SNR, nonlinearities in Si waveguides increase as well. The primary nonlinear effects are two-photon absorption (TPA), followed by absorption and refractive index change due to free carriers induced by TPA. These effects lead to signal-dependent loss and phase change – nonlinear effects responsible for harmonic distortions in photonic ADCs. The impact of these nonlinearities is most pronounced inside microring resonator filters because of resonant power enhancement. Fig. 2 shows the filter loss variations due to TPA versus pulse energy for a representative example of a dual-ring filter. These parameters were bandwidth = 25 GHz, channel spacing = 80 GHz, adjacent channel suppression = 32 dB, ring radius = 14 μm, free spectral range = 1 THz (enough to fit 12 channels), power enhancement factor = 10, and pulse duration inside the ring = 22 ps. The TPA coefficient was 0.5 cm/GW, Si waveguides were 600 nm wide and 105 nm tall, the effective TPA area [9] was calculated to be 0.1 μm^2. According to this plot, Si nonlinearities do not degrade performance at 8 bits and below; however, they quickly become a major source of distortions where 9 or more effective bits are desired. Note that although the drop loss variations shown in Fig. 2 are quite high, this loss includes a DC component, a smaller component varying at the frequency of the applied RF signal, and an even smaller component varying at twice the frequency. Only the latter component contributes to nonlinear distortions. Moreover, differential detection can completely eliminate this component, so that ADC performance will not be affected by TPA at all. Free carrier effects which lead to resonant frequency changes can be examined in a similar way; the results will be presented at the conference. Note that the impact of signal-dependent resonant frequency variations can be reduced by using the discrete time-to-wavelength mapping approach mentioned above, and making sure the bandwidth of the ring filters exceeds the bandwidth of the pulses in each channel.

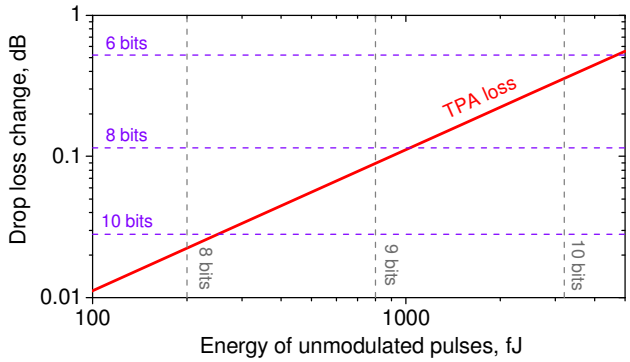

Fig. 2. Change in drop loss due to two-photon absorption as a function of energy of unmodulated pulses. Horizontal lines are the distortion levels corresponding to for 6, 8, and 10 effective bits, assuming 50% modulation. Vertical lines indicate unmodulated pulse energies required to obtain SNR-limited accuracy 8, 9, and 10 bits, determined as described above, again assuming 50% modulation index.

3. Modulator linearity

In a photonic ADC, low-jitter sampling occurs when an optical pulse train is modulated with the RF signal to be sampled. Most high-performance modulators with wide optical and electrical bandwidth are based on a Mach-Zehnder (MZ) structure, which has an inherently nonlinear (sinusoidal) transfer function, leading to a nonlinear relationship between the input RF signal and the samples at the output of the photonic ADC. This nonlinearity can be the single most important factor limiting the ADC dynamic range. One approach to overcome this problem is to apply a linearization algorithm in the digital domain at a post-processing step [5, 4]. An alternative solution is to develop a modulator with improved linearity [10], such as a linearized silicon modulator described below [11].

The layout of the linearized Si MZ modulator is shown in Fig. 3. The nonlinear phase shifts and voltage-dependent losses in the two arms are $\varphi(v)$ and $\alpha(v)$. The arms are biased at v_{DC} and the RF signal $v=v(t)$ is applied in a push-pull configuration, so that the total voltage at the top and bottom phase shifters is $v_{DC}\pm v$. The optical powers P_A and P_B at the top and the bottom outputs of the modulator biased at quadrature are given by

$$P_A = P_{in}\exp\left[-\frac{\alpha_A+\alpha_B}{2}\right]\sin^2\left(\frac{\pi}{4}+\frac{\varphi_A-\varphi_B}{2}\right)+\frac{P_{in}}{4}\left[\exp\left(-\frac{\alpha_A}{2}\right)-\exp\left(-\frac{\alpha_B}{2}\right)\right]^2, \quad (1)$$

$$P_B = P_{in}\exp\left[-\frac{\alpha_A+\alpha_B}{2}\right]\cos^2\left(\frac{\pi}{4}+\frac{\varphi_A-\varphi_B}{2}\right)+\frac{P_{in}}{4}\left[\exp\left(-\frac{\alpha_A}{2}\right)-\exp\left(-\frac{\alpha_B}{2}\right)\right]^2, \quad (2)$$

where $\varphi_A=\varphi(v_{DC}+v)$ and $\alpha_A=\alpha(v_{DC}+v)$ are the phase shift and loss in the top phase shifter, $\varphi_B=\varphi(v_{DC}-v)$ and $\alpha_B=\alpha(v_{DC}-v)$ are the phase shift and loss in bottom phase shifter, and P_{in} is the input power. Expansion of Eqs. (1, 2) into Taylor series gives

$$P_A = P_{in}e^{-\alpha_{DC}L}\left[1/2+(\varphi_1 L)v+\left(\alpha_1^2L^2-\alpha_2 L\right)v^2+\left(-2\varphi_1^3L^3/3+\varphi_3 L-2\varphi_1\alpha_2L^2\right)v^3+\ldots\right], \quad (3)$$

$$P_B = P_{in}e^{-\alpha_{DC}L}\left[1/2-(\varphi_1 L)v+\left(\alpha_1^2L^2-\alpha_2 L\right)v^2-\left(-2\varphi_1^3L^3/3+\varphi_3 L-2\varphi_1\alpha_2L^2\right)v^3+\ldots\right], \quad (4)$$

where Taylor series expansion of the phase and loss has been used, $\varphi(v_{DC}+v)=\left(\varphi_{DC}+\varphi_1 v+\varphi_2 v^2+\varphi_3 v^3+\ldots\right)L$, $\alpha(v_{DC}+v)=\left(\alpha_{DC}+\alpha_1 v+\alpha_2 v^2+\alpha_3 v^3+\ldots\right)L$; L is the phase shifter length. One can see that cubic term is completely canceled in both modulator outputs if $2\varphi_1^3L^2/3+2\varphi_1\alpha_2L-\varphi_3=0$. Although the quadratic term cannot be cancelled simultaneously with the cubic term in both outputs, it can be eliminated using differential detection, which produces the difference (P_A–P_B). Alternatively, the quadratic term can be eliminated in one of the MZ outputs by adjusting the MZ bias point to introduce quadratic nonlinearity which cancels that of (3) or (4).

To confirm that linearization predicted by analytical analysis is possible and happens at realistic modulation parameters, an example of a silicon diode, shown in Fig. 3(b) [12], has been considered. Its response has been found numerically using Synopsys' Sentaurus software suite and a finite-difference optical mode solver. A single-frequency sinusoidal signal applied to the RF input of the modulator has been considered. The levels of harmonic distortions at the output of the silicon modulator are shown in Fig. 4 for three different diode lengths and compared to the third harmonic distortion of a conventional MZ modulator with similar modulation depth. It is clear that in all three cases the linearity of the silicon modulator is considerably improved. The phase shifter lengths are several hundreds of microns, which is typical for MZ silicon modulators reported in the literature.

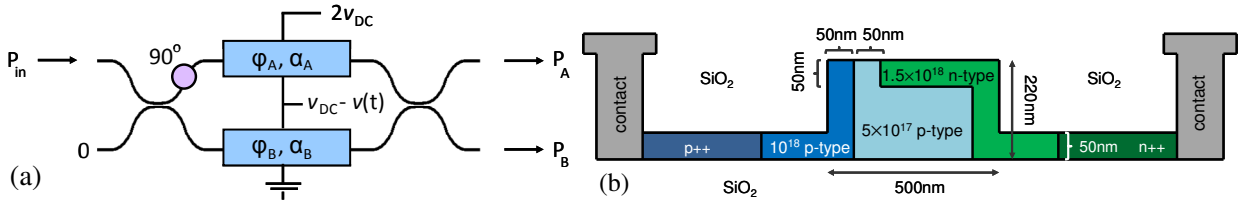

Fig. 3. (a) The configuration of the MZ modulator studied in this work. The two arms have identical nonlinear phase shifters biased with DC bias voltage v_{DC}, driven in a push-pull mode with the RF signal $v(t)$. The 90° phase shifter biases the MZ modulator at quadrature. (b) An example cross-section of the reverse-biased Si diode phase shifter considered in this work.

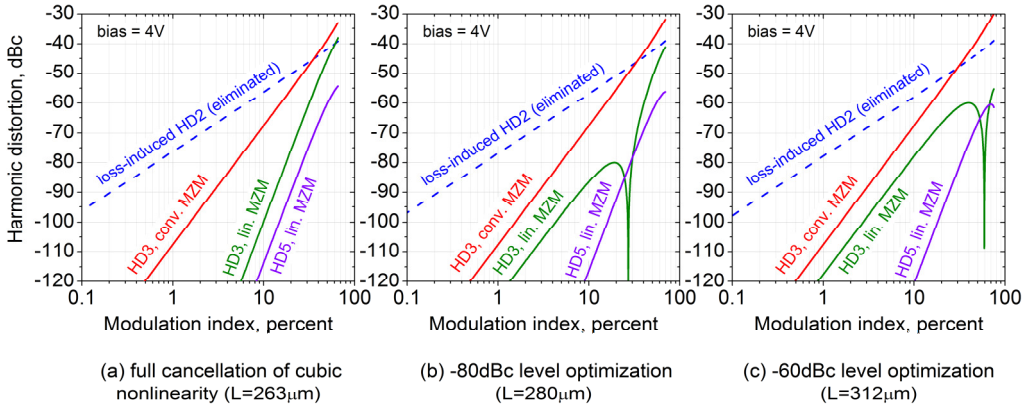

Fig. 4. Harmonic distortions in the linearized Si modulator and a conventional MZ modulator vs. modulation index. The curves "HD3, lin MZM" and "HD5, lin MZM" are the 3rd and 5th harmonic distortions in the linearized Si modulator, while the curve "HD3, conv. MZM" is the 3rd harmonic distortion in a conventional MZ modulator. The curve "loss-induced HD2" illustrates the 2nd harmonic distortion due to voltage-dependent loss, which can be eliminated by adjusting the MZ bias or using differential detection. The length is selected (a) to completely eliminate the cubic nonlinearity, (b) to achieve the largest modulation depth while keeping HD3 below the -80dBc level; (c) the same for -60dBc level. The Si diode bias voltage was -4V.

5. Acknowledgments

This work was sponsored by the Defense Advanced Research Projects Agency (DARPA) EPIC Program under contract W911NF-04-1-0431 and United States Air Force Office of Scientific Research (AFOSR) grant FA9550-10-1-0063. C. Sorace would like to acknowledge support from a Graduate Research Fellowship of the National Science Foundation.

6. References

1. G. C. Valley, "Photonic analog-to-digital converters," *Opt. Express* **15**, 2007, pp. 1955-1982.

2. M. Y. Frankel, J. U. Kang, and R. D. Esman, "High performance photonics analogue digital converter," *Electronics Letters* **33**, 1997, p. 2096.

3. A. Yariv and R. Koumans, "Time interleaved optical sampling for ultra-high speed A/D conversion," *Electronics Letters* **34**, 1998, pp. 2012-2013.

4. J. U. Kang and R. D. Esman, "Demonstration of time interweaved photonic four-channel WDM sampler for hybrid analogue-digital converter," *Electronics Letters* **35**, 1999, pp. 60-61.

5. R. C. Williamson, R. D. Younger, P. W. Juodawlkis, J. J.Hargreaves, J. C. Twichell, "Precision calibration of an optically sampled analog-to-digital converter," 2003 Digest of the LEOS Summer Topical Meetings, 14-16 July 2003, pp. MC4.2/22- MC4.2/23.

6. S. Gupta and B. Jalali, "Time warp correction and calibration in photonic time stretch analog-to-digital converter," *Opt. Lett.*, **33**, 2008, p. 2674.

7. G. Sefler, J. Chou, J. Conway, and G. Valley, "Distortion Correction in a High-Resolution Time-Stretch ADC Scalable to Continuous Time," *Journal of Lightwave Technology* **28**, 2010, pp. 1468-1476.

8. G.C. Valley, "Photonic analog-to-digital converters: fundamental and practical limits," *Proc. SPIE* **5618**, 2004, pp. 96-106.

9. C. Koos, L. Jacome, C. Poulton, J. Leuthold, and W. Freude, "Nonlinear silicon-on-insulator waveguides for all-optical signal processing," *Opt. Express* **15**, 2007, pp. 5976-5990.

10. C. H. Cox, III, *Analog optical link: Theory and practice*, Cambridge, U.K, Cambridge University Press, 2004.

11. A. Khilo, C. M. Sorace, and F. X. Kärtner, "Broadband Linearized Silicon Modulator," *Opt. Express* **19**, 2011, pp. 4485-4500.

12. S. J. Spector, C. M. Sorace, M. W. Geis *et. al.*, "Operation and Optimization of Silicon-Diode-Based Optical Modulators," *IEEE J. Sel. Top. Quantum Electron*. **16**, 2010, pp. 165-172.